Fabricating Atom-Sized Gaps by Field-Aided Atom Migration in Nanoscale Junctions

Ran Liu,[1] Jun-Jie Bi,[1] Zhen Xie,[1] Kaikai Yin,[2] Dunyou Wang,[1] Guang-Ping Zhang,[1] Dong Xiang,[2,*] Chuan-Kui Wang,[1,†] and Zong-Liang Li[1,‡]

[1]*School of Physics and Electronics, Shandong Normal University, Jinan 250014, China*
[2]*Key Laboratory of Optical Information Science and Technology, Institute of Modern Optics, College of Electronic Information and Optical Engineering, Nankai University, Tianjin 300071, China*

(Received 13 November 2017; revised manuscript received 4 January 2018; published 16 May 2018)

The gap sizes between electrodes generated by typical methods are generally much larger than the dimension of a common molecule when fabricating a single-molecule junction, which dramatically suppresses the yield of single-molecule junctions. Based on the *ab initio* calculations, we develop a strategy named the field-aided method to accurately fabricate an atomic-sized gap between gold nanoelectrodes. To understand the mechanism of this strategy, configuration evolutions of gold nanojunction in stretching and compressing processes are calculated. The numerical results show that, in the stretching process, the gold atoms bridged between two electrodes are likely to form atomic chains. More significantly, lattice vacant positions can be easily generated in stretching and compressing processes, which make field-aided gap generation possible. In field-aided atom migration (FAAM), the external field can exert driving force, enhance the initial energy of the system, and decrease the barrier in the migration path, which makes the atom migration feasible. Conductance and stretching and compressing forces, as measurable variables in stretching and compressing processes, present very useful signals for determining the time to perform FAAM. Following this desirable strategy, we successfully fabricate gold nanogaps with a dimension of 0.38 ± 0.05 nm in the experiment, as our calculation simulates.

DOI: 10.1103/PhysRevApplied.9.054023

I. INTRODUCTION

For the last two decades, we have witnessed the rapid progress of single-molecule technologies and molecular electronics [1–9]. It is known that fabricating a nanoscale gap from a nanowire is the prerequisite step for constructing a single molecular junction [10–23]. However, it is still a hard task to accurately generate an atom-sized nanogap and steadily control the tip configurations of the electrodes [24–27]. For example, the nanogap is normally larger than 5 nm, whether by the electromigration method or by the reactive-ion-etching method [28,29], which greatly hinders the yield of single-molecule-device fabrications. To overcome the low-yield problem, strategies must be developed to accurately form atom-sized gap using nanowire. Fortunately, when nanowire is stretched, the conductance trace often shows stepwise features, which is a pronounced character that may be utilized to accurately form an atom-sized gap. Especially in the process of stretching metal nanowire, the one-G_0 ($G_0 = 2e^2/h$) step in the conductance trace indicates that the nanowire will be broken upon a further elongation [30–33]. However, if one breaks the nanowire directly by stretching, the gap size is generally from one to several nanometers at random due to the relaxation of the gap interface after breaking. This random gap size is often larger than the general dimension of a single molecule, which consequently results in the low yield of the single-molecule junction [34]. The mechanically controllable break junction (MCBJ) technique has the unique advantage of accurately fabricating nanogaps with atom scales because the gap can be adjusted at 0.1 nm accuracy or even at picometer accuracy using the MCBJ technique [5,34]. However, it is inconvenient to adjust distance by moving electrodes in the circuit integration. Thus, in order to overcome this difficulty, we suggest that the bias voltage added to the electrodes can be applied to migrate metal atoms near the interface [35–40] to generate nanogaps. Specifically, we recently found that the atoms at the contact tip of the metal junction can be removed one after another from the constriction and ultimately induced a break by bias voltage [34], which opens a window to accurately fabricate an atom-sized gap by nanowire with the MCBJ technique without further moving the electrodes.

In order to clarify the formation of an atom-sized gap by field-aided atom migration (FAAM), in this work, we investigate the configuration evolution of gold nanojunctions during stretching and compressing processes and field-inducing processes by *ab initio* calculations. The most

*xiangdongde@126.com
†ckwang@sdnu.edu.cn
‡lizongliang@sdnu.edu.cn

possible configurations of the gap interface are described in the evolution process and the minimum gap size of the system is investigated. It is found that, even though there are different kinds of breaking probabilities, the gap interfaces can mainly be categorized into two types. The vacant positions generated in the stretching processes make FAAM feasible. When a certain voltage is applied to the stretched nanowire, the migration of the atoms creates a gap with a relatively accurate dimension of only a one-atom size. Employing energy traces and force traces plotted in the atom migration processes, the underlying mechanisms of generating nanogaps with an accurate one-atom dimension with the FAAM method are clarified. This nanogap generation scheme is confirmed by our innovative MCBJ experiments.

II. THEORETICAL METHOD AND COMPUTATIONAL DETAILS

The stretching and compressing processes of gold nanojunctions and the formation of gold nanogaps are simulated at *ab initio* levels. In the simulation, a gold nanojunction is constructed as shown in Fig. 1. Since only the neighboring Au layers have obvious interactions with each other and the interface configuration in the junction-breaking and gap-forming process mainly relates to several atoms near the interface of the gold junction, in the simulation, only the atoms in the dashed rectangle are considered. The reliability of the results is validated by a few larger systems with more layers of Au atoms which consume significant computational cost for each calculation. The stretching or compressing forces are exerted on the outer gold layers during the simulation of the stretching and compressing processes of the gold nanojunction. Specifically, for each stretching distance, the forces are exerted on layer $L3$ and layer $R3$ (see Fig. 1) by fixing the two layers, while the inner layers are relaxed to allow for geometric optimization in the calculation. Here, the stretching distance (or electrode distance, denoted as D) is defined as the distance between layer $L3$ and layer $R3$ in Fig. 1.

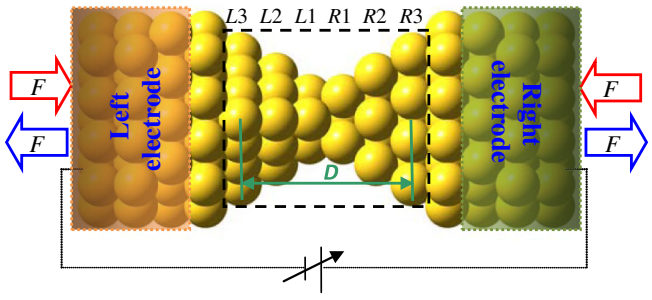

FIG. 1. The schematic structure of the gold nanojunction. The structure shown in the rectangular frame represents the initial configuration of the atomic gold wire before stretching and compression.

The stretching and compressing processes of the system are simulated by adjusting the electrode distance (D) between layer $L3$ and layer $R3$ step by step. For each step, the positions of relaxed atoms that are just optimized in the last step are taken as the initial geometry to perform further geometric optimization [41,42]. In this way, the stretching and compressing processes are calculated at Becke, three-parameter, Lee-Yang-Parr level with the Lanl2DZ basis set in GAUSSIAN03 packages [43]. The conductance of the gold junctions in different stretched states is calculated by using the nonequilibrium Green's function (NEGF) method combined with density-functional theory implemented in the TranSIESTA module of the SIESTA package. In the NEGF calculations, the gold junctions are divided into three regions, i.e., left electrode, scattering region, and right electrode (see Fig. 1). According to the Landauer-Buttiker formula [44], the current with different bias for the molecular junction is written as

$$I = \frac{2e}{h}\int T(E,V)[f(E-\mu_L) - f(E-\mu_R)]dE, \quad (1)$$

where $T(E,V)$ is the transmission probability. μ_L and μ_R are the electrochemical potentials of the two electrodes. After current calculations, the differential conductance is obtained by using $G = \partial I/\partial V$. In the calculation, the improved Troullier-Martins-type norm-conserving pseudopotentials are used to describe the core electrons of Au atoms. A single-ζ plus polarization basis set is employed for the valence shell electrons of Au atoms. The Perdew-Burke-Ernzerhof generalized-gradient approximation is adopted for the exchange-correlation functional [45].

III. RESULTS AND DISCUSSION

Fabricating an atom-sized gap using a gold nanowire requires highly accurate experimental technology. The electrodes should be stretched and compressed repeatedly at picometer accuracy, which can be fulfilled by the differential-screw-based mechanically controllable break-junction technology developed by us recently [34]. In order to fabricate a nanogap with high yield and high efficiency, a series of stretching and compressing processes of gold nanojunctions are simulated theoretically. Using the simulation, the probable interface configurations, the mechanics information, and the conductance signals, which are very significant to the fabrication of atom-sized gap, are discussed.

Considering that the probable interface configurations produced in the experimental fabrications often vary, for they are generally related to the stretching and compressing velocity, we adopt different step lengths for the stretching and compressing of the gold junction in the theoretical simulation, which can roughly present the effects of different stretching or compressing velocities. Since

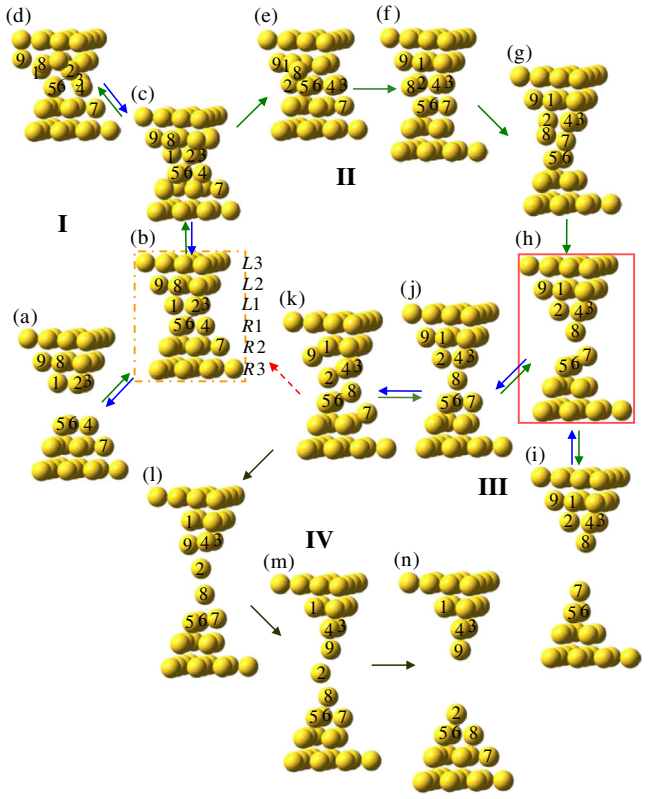

FIG. 2. The evolution of system configuration and the rebuilding of the gap interface during the breaking and recontact processes. We display four possible processes for the system being stretched and recontacted, denoted as process I [(a) ↔ (b) ↔ (c) ↔ (d)], process II [(e) → (h)], process III [(i) ↔ (h) ↔ (j) ↔ (k)], and the semistable process IV [(k) → (n)].

different interface configurations can be produced by adopting different stretching or compressing step lengths in the simulation—no matter which initial geometry is applied—we begin our calculations from a relatively regular probable geometry, as shown in Fig. 2(b), which can be formed with large probability by repeated breaking and recontact operations in the experiment for its stable structure.

A. Breaking and recontact simulation

Figure 2 shows several probable configuration evolutions of the gold nanojunction in different stretching or compressing processes. In the figure, process I [i.e., (a) ↔ (b) ↔ (c) ↔ (d)] can be seen as a reversible process for which the electrode distance changes only 0.02 nm for each step. In process I, configuration (b) is close to the standard lattice structure with an electrode distance of 1.16 nm, which has the lowest ground-state energy of all the configurations used in our simulations. Although the arrangement of the Au atoms in the middle two layers is apparently deformed when the electrode distance is compressed to 0.98 nm [configuration (d)], by reversed stretching from configuration (d), the configuration of the gold junction is still turned back to configuration (c) and then to configuration (b). It should be mentioned that a higher energy barrier needs to be surmounted for the compressing process from configuration (c) to (d) than for the reversed stretching process from configuration (d) to (c) [see Fig. 3(a)].

However, from configuration (c) ($D = 1.06$ nm), if we compress the gold junction with a faster velocity, i.e., each electrode moves 0.02 nm to compress the gold junction to $D = 0.98$ nm [Fig. 2(e)], an absolutely different stretching process takes place. Figure 2(e) shows that, with the compression, five atoms in the middle two layers are rearranged into one new layer, while atom 1 is plunged into layer $L2$, with atom 8 being squeezed out. Because of the rearrangement of the new layer, the gold junction is converted into an irreversible lower energy state [Fig. 3(a)]; thus, the stretching operation results in a new process from

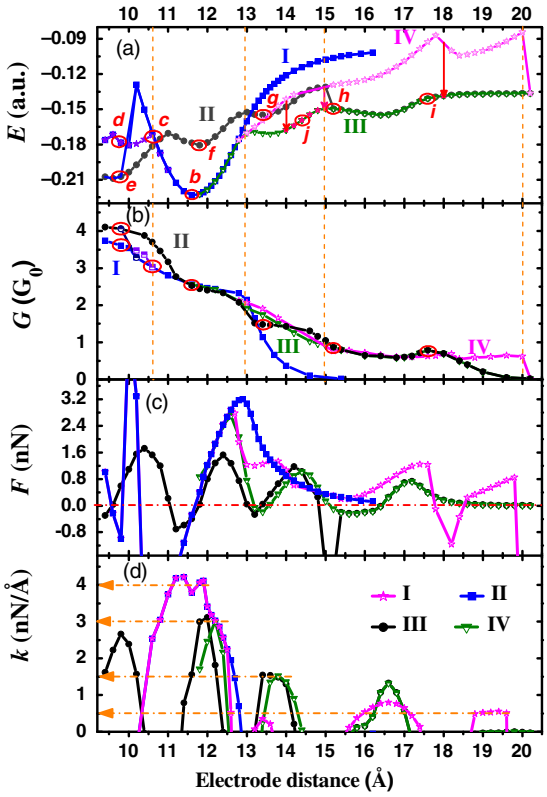

FIG. 3. The evolution of the energy (E), conductance (G), force (F), and differential stiffness factor (k) of the gold junction in the compression processes I and III and the stretching processes II and IV. (a) Ground-state-energy curves of the system during different evolution processes. (b) Steplike decreases of conductance traces during these four processes. The quantized steps are presented with a step difference of approximately $1G_0$ when the electrode distance increases. (c) The stretching force that the system experiences during these four processes. (d) Curves of the differential stiffness factor, which corresponds to the energy valleys in (a) and the conductance steps in (b).

configurations (e) to (h) (denoted as process II). For process II, with the stretching of the electrode, atom, 2, 3, 4, and 8 form the new layer $L1$, and atoms 5, 6, and 7 form the new layer $R1$ [Fig. 2(f)], where atom 8 came from layer $L2$, atom 4 came from layer $R1$ and atom 7 came from layer $R2$ in the initial configuration [configuration (b)]. It should be mentioned that the electrode distance of configuration (f) is 1.16 nm, which is the same as that of configuration (b). To further stretch the gold junction, atoms 7 and 8 move into the separation between layer $L1$ and layer $R1$ [configuration (g), $D = 1.34$ nm], and, finally, the gold junction is broken between atoms 8 and 7 with the electrode distance of 1.74 nm [Fig. 2(i)]. Process II is not reversible from configuration (g) to (h) ($D = 1.52$ nm) because, when atom 8 enters the gap between atoms 2 and 7, an atom chain consisting of atoms 9, 2, 8, and 7 is formed, which makes the energy of the gold junction decrease sharply [Fig. 3(a)]. Thus, compressing the junction from configuration (h), it is easier to push atom 7 to glide on the edge of the junction than it is for atom 8 to be resqueezed out, which results in another process (denoted as process III).

Figure 2 shows that, with the compression from configuration (h), atom 8 pushes atom 7 to layer $R1$ [configuration (j), $D = 1.44$ nm], and layer $L1$ then pushes atom 8 to layer $R1$ and, at the same time, pushes atom 7 to layer $R2$ [configuration (k)]. Meanwhile, atoms 5, 6, and 8 attract atoms 2 and 9 and deviate from layers $L1$ and $L2$, respectively [configuration (k), $D = 1.28$ nm]. The approximately standard lattice formation configuration (b) is achieved again if the gold junction is further compressed to $D = 1.16$ nm, but the atomic arrangement is obviously different from configuration (b). Process III is a reversible process. When each gold electrode is stretched with 0.02 nm for each step from configuration (k), the junction goes over configurations (j) and (h) until at last being broken with configuration (i). The evolutions of processes I, II, and III show that, although the structure of the junction is deformed and even the atoms in the junction are rearranged differently in different stretching and compressing processes, the standard lattice arrangement is still the most probable choice for the gold junction at the proper electrode distance.

In process III, configuration (k) is a very interesting configuration. In this configuration, because of the attraction of atoms 8 and 7, atom 2 deviates from layer $L1$ and atom 9 deviates from layer $L2$. In fact, the geometric optimizations show that atoms 9, 2, 8, and 7 attract each other relatively more strongly than with other atoms, which seem to be forming a single-atom chain in configurations (h) and (j). Because these stronger attractions still remain in the stretching or compressing process, in the geometric optimizations, the atoms in this chain generally move together. Hence, in configuration (k), when atom 8 is squeezed to move into layer $R1$ and atom 7 to move into layer $R2$, atoms 2 and 9 deviate from layer $L1$ and $L2$, respectively, by the attraction of atoms 8, 5, and 6. Considering the relative stronger attractions between atoms 9, 2, 8, and 7 in configurations (h), (j), and (k)—especially in configuration (k)—the distance between atom 9 and layer $L3$ is enlarged to be similar to the distance between atom 7 and layer $R3$, we are very interested in whether or not a real single-atom chain can be stretched out between two electrodes? To attempt to form a single-atom chain by *ab initio* simulations, we first stretch each electrode with small steps, such as 0.01 or 0.02 nm for each step. The simulation shows that, when the electrode distance reaches 1.44 nm, the atom chain consisting of atoms 9, 2, 8, and 7 easily slips to be close to one electrode as configuration (j), (h), or (i). However, when we stretch the junction with large steps, such as when each electrode moves 0.03 or 0.04 nm for each step, atoms 9, 2, 8, and 7 stay in the center region and a single-atom chain gradually emerges between the two electrodes as configurations (l) and (m) (see process IV in Fig. 2). When the electrode distance is above 1.82 nm, a gold atom chain in the length of three atoms can be stretched out. The longest stretching distance of process IV is 2.02 nm; further stretching results in the breaking of the gold junction shown in configuration (n). It can be seen that configurations (n) and (e) are the same configuration if one rotates the system by 180° with respect to the center of the system. In fact, the atom chain consisting of atoms 9, 2, 8, and 7 can be seen as gliding on the Au(100) surface when the junction is stretched in process IV; hence, the single-atom chain seems relatively stable in processes III and IV. Our simulation shows that to produce a single-atom chain is not an easy task because the gold junction is in a high-energy state in the stretching process, which can be easily seen by comparing the energy of process IV with process III from Fig. 3(a).

B. Signals in conductance and force curves for fabricating atom-sized gaps

Conductance and stretching or compressing forces can give useful information for judging the configuration of the junctions which can be obtained by experiment. Figure 3(b) shows the conductance traces of the gold junctions in the four stretching or compressing processes. Because the number of connected atoms in the breaking region of a gold nanojunction decreases one by one in the stretching process, the conductance traces show stepwise features for all four of the processes which are often presented in the experimental probes [33,34,46–48]. There are two especially significant characteristics for the stepwise conductance traces. The first one is that the conductance steps generally appear at the valley position of the energy curve. The reason is that when the gold junctions are stretched to a relatively equilibrium state, the configuration of the junction changes slightly with the variation of the electrode distance. Thus, the conductance of the junction generally shows insensitivity to the change of the electrode distance

in the vicinity of the equilibrium state of the junction, which results in the conductance traces showing the plateau features. On the contrary, when distinct changes take place for the configuration of the gold junction, the energy curve generally shows peak features. The conductance is very sensitive to the change of electrode distance in the vicinity of the peak energy point; i.e., swift or sharp changes often take place for the conductance traces. The second characteristic is that most of the conductance traces show wide one-G_0 steps, except in the case of process I. In process I, the gold junction breaks from the standard lattice structure with a three-atom connection [configuration (b)], so the last conductance step is a higher plateau with a conductance of about $2.5G_0$ in our calculated conductance trace. However, for the other processes, the junction is generally connected by one atom [configuration (h)] or single-atom chain [configuration (m)] before the junction is broken, which results in one-G_0 steps in the conductance traces. According to the characters of conductance traces, in the experiment, when a one-G_0 step emerges, one can stop the stretching operation and fix the electrode. Then proper bias voltage can be applied to the gold junction to move the atoms away from the connection region to produce the atom-sized gaps.

Generally, the one-G_0 plateau is about 0.2–0.5 nm in width; thus, the accurate electrode distance to stop the stretching operation cannot be directly determined by the conductance trace only. Then the stretching force is another important measurable quantity which can be applied to determine when the electrode should be fixed, and the bias voltage should be added. In order to understand the important role of the stretching force in the fabrication of the nanogaps, applying $F = \Delta E/\Delta D$, we calculate the stretching or compressing forces of the four processes as shown in Fig. 3(c), where positive values indicate stretching forces, while negative ones represent compression forces. The figure shows that, due to the break from the three-atom connection, the broken force of process I is about 3 nN, which is much larger than those of the other processes. For processes II, III, and IV, the peak force values for the configuration variations are all about 1.5 nN. However, only about 0.9 nN is required for the junction to finally break from one-atom contact. It should be mentioned that, when the conductance reaches $1G_0$ in the stretching process, zero force indicates that the gold junction is at equilibrium state, with one atom or a single atom chain connected between two electrodes.

Additionally, if we define $k = \Delta F/\Delta D$ as the differential stiffness factor (DSF) of the gold junction, we can obtain more significant information from the peak values of the DSF. Figure 3(d) shows that the largest stiffness factor for process I is about 4.0 nN/Å, which occurs in configuration (b). The peak value of the DSF for process II is about 3.0 nN/Å, which occurs in configuration (f), with an electrode distance of about 1.2 nm. While, at 1.38 nm, the DSFs are about 1.5 nN/Å in process II and process III. In process IV, the DSFs for configurations (l) and (m) are about 1.0 nN/Å and 0.5 nN/Å, respectively. It can be seen that, when a one-atom connection or a single-atom-chain connection forms, the stiffness factor is not more than 1.5 nN/Å. Specifically, if a single-atom chain forms and glides on the tip surfaces in the stretching process, the stiffness factor is only about 0.5–1.0 nN/Å. The DSFs calculated by us are very consistent with the measurement of Aradhya *et al.* [31]. The decrease of DSF peak values is related to the decrease of Au atoms that connect between the two electrode tips in these configurations. Hence, one can see that the DSF is a significant quantity for judging the number of gold atoms connected between the two electrode tips, which cannot be solely judged by force curves in the stretching processes. Obviously, with further stretching of the system, the electrode distance increases more easily under the external force; i.e., when the Au atom chain is pulled out, the electrode distance increases faster than any other equilibrium configurations before the junction is broken. Thus, because of the relaxation in the stretching process and after the junction is broken, the gap size is often unpredictable if it is fabricated only by stretching the gold junction, especially when there is a single atom chain being pulled out [49].

C. Field-aided atom-sized gap fabrication

Field-induced atom migration applied with the MCBJ technology is the most available strategy to avoid relaxation after the junction is broken and fulfill the accurate fabrication of an atom-sized gap because of the way in which one can fix the electrodes at any selective distance before the junction is broken by stretching. In Fig. 2, one can see that the configurations from (j) ($D = 1.44$ nm) to (h) ($D = 1.52$ nm) in process III, and the configurations in the evolution path from configuration (h) to configuration (i) before the junction is broken seem to be the ideal configurations to produce an one-atom-sized gap. This is the case because there is only one atom in the contact region between the two electrodes, and the vacant position beneath atom 7 is very suitable for atom 8 and atom 7 to locate when they move away from the contact point. Specifically, these configurations are in a regime for conductance that decreases from a higher plateau to the $1\,G_0$ plateau, and the stretching force decreases from the peak value (about 1.2–1.5 nN) to zero. Thus, both the conductance curve and the force curve show excellent character for determining the time to fix the electrodes and perform field-induced atom migration. Additionally, the system energy of process III is obviously lower than those of other processes when the electrode distance is up to 1.35 nm, which enhances the probability of process III taking place.

The *ab initio* calculations show that, for the junctions from configurations (j) to (h), atom 8 possesses positive

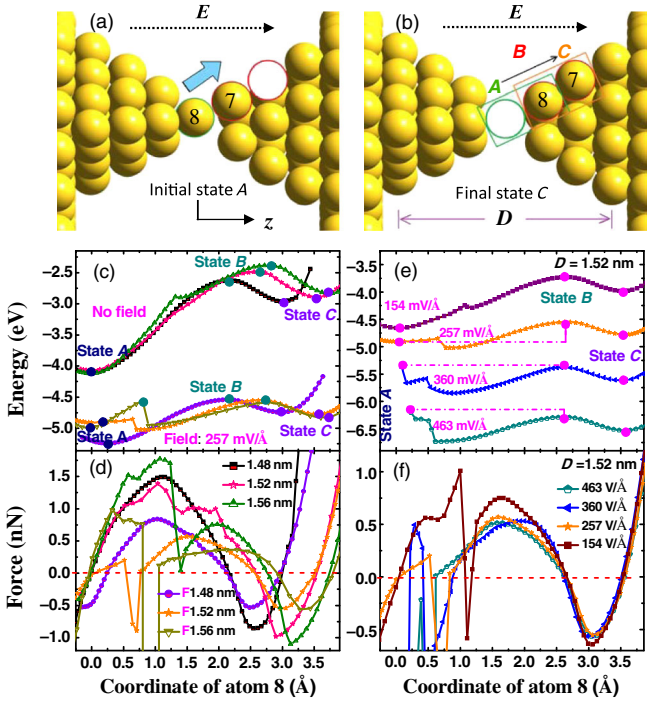

FIG. 4. The schematic process of field-aided gap generation and the corresponding evolution of system energy and atom migration force. (a) The initial state of the atom migration process. (b) The atom migration process under an external electric field. After the migration of atoms 7 and 8 induced by external field, a single-atom-sized gap is formed between two electrodes. (c) Ground-state energies, as functions of migration positions with or without an external field, for gold junctions with electrode distances of 1.48, 1.52, and 1.56 nm. (d) The corresponding migration force for atoms 7 and 8 migrating to different positions. (e) Energy curves in the atom migration processes for the junctions in fields of 154, 257, 360, and 463 mV/Å, with an electrode distance of 1.52 nm. (f) The corresponding migration force for the migration processes shown in (e).

charges of more than 1.0*e*, while atom 7 is little charged. Thus, it is more possible that, in field-induced atom migration, the applied field drives atom 8, and consequently atom 7 migrates ahead. Figures 4(a) and 4(b) show the most probable atom migration process, where *A* represents the initial state of atoms 7 and 8, *C* represents the final state of atoms 7 and 8, and *B* is the transition state. The single-point energy and corresponding force for the atoms migrating to different positions along the electrode surface with or without an external field are shown as Figs. 4(c) and 4(d), where the strength of the applied field is 257 mV/Å. There are three sets of energy traces which correspond to junctions with electrode distances of 1.48, 1.52, and 1.56 nm, respectively.

Figure 4(c) shows that, without an external field, there is a large energy difference of about 1.1–1.3 eV between initial state *A* and final state *C*. When the field is applied, the energy difference for the junction with an electrode distance of 1.48 nm decreases to 0.5 eV, with a 0.7-eV barrier between initial state *A* and transition state *B*. For the distance of 1.52 nm, however, the energy difference decreases to only about 0.1 eV, with a barrier of about 0.3 eV. For a distance of 1.56 nm, the energy difference between state *A* and state *C* is about 0.2 eV, with a barrier of about 0.5 eV between state *A* and state *B*. Moreover, for distances of 1.52 and 1.56 nm, the energy shows a sharp decrease when the junction is broken in the external field for atom 8 in the vicinity of 0.7 and 0.8 Å. Thus, the result shows that the junction with an electrode distance of 1.52 nm is more suitable for the atom migration than the junction with distances of 1.48 and 1.56 nm. Figure 4(d) shows that the force for atom 7 and atom 8 migrating away from state *A* together is only about 0.5 nN, with the field being applied for the junction with an electrode distance of 1.52 nm. However, it is about 1.5 nN for the system without a field. Thus, the applied electric field weakens the action of the junction on the migrating atoms.

Obviously, after field-induced atom migration, the geometry of the gold junction is similar to configuration (a). If the electrode distance is 1.52 nm, the gap formed after atom migration is about 0.36 nm. It should be mentioned that, when the electrode distance is shorter than 1.48 nm, the migration of atom 8 can attract atoms 2 and 9 together, thus, the atom-sized gap is not produced for the gold junction with a shorter electrode distance. Moreover, when the electrode distance is larger than 1.56 nm, the barrier for atom 8 breaking from atom 2 is higher than 0.5 eV, even under a field of 257 mV/Å. Specifically, the force for atom 8 to be overcome is up to 1.0 nN, which is hard to overcome even though atom 8 is positive charged. Thus, based on the calculation, one can see that the size of the gap fabricated by field-induced atom migration mainly falls into a most probable regime with a dimension of 0.32–0.40 nm, which is confirmed by our experiment (Fig. 5).

Figures 4(e) and 4(f) show the energy and the force curves for the gold junctions at different values of the external electric field with an electrode distance of 1.52 nm. These figures show that, with the increase of the field, the energy of the initial state of the system increases relative to that of the final state and gradually exceeds the energy of the final state, which can dramatically promote atom migration. When the value of the electric field increases to 360 mV/Å, the energy of initial state *A* is approximately equal to that of transition state *B* [Fig. 4(e)]. As the field increases to 463 mV/Å, the energy of state *A* is 0.12 eV larger than that of state *B*. Thus, with the increase of the field, the migration of atoms 7 and 8 becomes easier and easier. It is noticeable that there always exists an energy barrier in the migration path at point *B* [Fig. 4(e)], which seems to be an obstacle for the migrations of atoms 7 and 8. However, this energy barrier is positive for atom migration because this kind of barrier can prevent electrode tips from avalanche-type deforming and rearranging [34,50]. Moreover, when the barrier is not more than 0.3 eV, it

can be easily overcome with the help of atomic vibration at room temperature.

D. Experimental confirmations for the field-aided atom-sized gap fabrication schemes

In order to confirm our theoretical scheme, we fabricate several gold nanojunction chips employing MCBJ technology. The work principle of MCBJ is shown in Fig. 5(a). A MCBJ setup consists mainly of three parts: a flexible substrate containing a suspended metal wire with a nanoconstriction, a push rod, and a counter support. The metal wire is fabricated by standard electron-beam lithography, and the movement of the push rod is controlled by piezoelectric actuator. Owing to the mechanical configuration of the three-point apparatus, a long vertical movement (ΔZ) of the push rod causes only a short elongation of the nanoconstriction (ΔX). Here, an attenuation factor $r \sim 2 \times 10^{-6}$ ($r = \Delta X/\Delta Z$) can be obtained with our setup, which means we can stretch the nanoconstriction with subangstrom accuracy [51,52]. When the push rod exerts a bending force on the substrate, the constriction part undergoes the largest stretching force, which reduces the cross section of the nanoconstriction. We precisely stretch the metal wire at a speed of 0.1 Å/step, and the conductance of the metal wire is monitored simultaneously. Once the monitored conductance is close to $1G_0$, the push rod is fixed by holding the piezoelectric actuator. It is noteworthy that the conductance is stable—without obvious fluctuations over several hours—when the push rod is fixed.

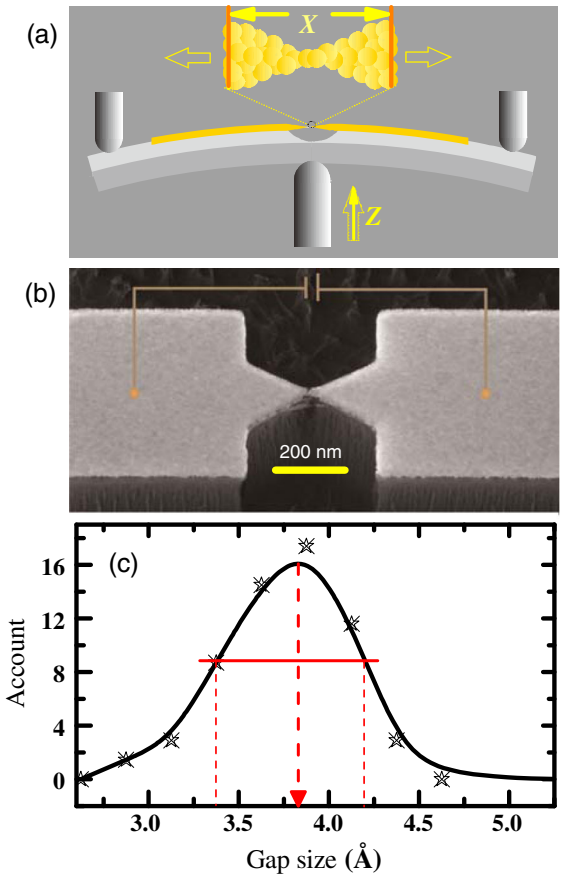

FIG. 5. Working principle and experimental data for the generation of an atom-sized gap. (a) Working principle of the MCBJ setup. A suspended metal bridge with a constriction is fabricated on the substrate. The substrate is fixed on a three-point bending apparatus. The movement of the push rod in the Z direction causes an elongation of the constriction in the X direction. The elongation of the constriction can be precisely controlled by the bending of the substrate. (b) SEM image of the chips after a break of the nanobridge. (c) The distribution of gap size after a break of the gold nanojunctions. The gaps are fabricated by field-induced atom migration from junctions with one G_0 state.

Subsequently, a linear increased bias voltage is applied to drive the atoms away from the contact regime of the junction to produce an atom-scale gap. Once a conductance jump ($> 0.2G_0$) is detected, a linear decrease in the voltage is triggered immediately and controlled by the feedback system. When the atom bridging the nanowire is removed from the constriction, the current jumps to the tunnel regime ($G \ll 1G_0$), indicating the complete breaking of the nanowire and that an atomic scale gap has been generated. One merit of the MCBJ technique is that the gold bridge can be repeatedly broken and recontacted by the control of the substrate; thus, different samples can be formed through these repeated processes. In the experiments, we examine five different chips, and each chip produces approximate 15 gaps. Based on the detected conductance and the attenuation factor of the MCBJ setup, we can determine the sizes of the nanogaps [53,54], which are shown in Fig. 5(c). This figure shows that, because of the field-induced atom migration, the most probable size of the gaps is 0.38 ± 0.05 nm, which corresponds to the dimension of a one-gold-atom gap and agrees well with our theoretical simulations. Thus, the atom-sized gaps are successfully fabricated with high yields by the aids of field-induced atom migration.

One challenge for the nanogap fabrication is the excessive Joule heating under high current intensity, which may result in an unexpected melt of the gold junction. In order to avoid the excessive Joule heating, different strategies had been put forward [55–57]. Fortunately, excessive Joule heating can also be avoided in our experiment due to the following facts. (1) Employing the MCBJ technique, the metal wire can initially be stretched to a single atom nanobridge. Therefore, the displacement of an atom near the bridge can be triggered under a small bias voltage (50–100 mV is observed in our experiments), which is a much lower value than the threshold voltage (0.5–1.0 V) needed in a typical electromigration experiment employing bulk metal wires that are dozens of nanometer in diameter. (2) The heat dissipation rate is much faster in the nanojunction (a few atoms in diameter) due to the relatively larger surface area compared to the bulk metal wire. Thus,

excessive heating can be suppressed in our experiments. (3) In order to reduce the heating effect, a middle level vacuum with approximately 0.1 bar of argon is applied when we perform the experiments, through which the high excited vibration modes can be suppressed and the excessive heating can be reduced.

Compared to the effect of the electric field, which normally moves the atoms in a specific orientation, the excessive heating related to the high excited vibration modes generally drives atoms in random directions. However, a suitable amount of heating or vibration can also provide useful energy for atoms to surmount the potential barriers in the migration path. Thus, with the help of the vibration, the actual field needed to move the atoms is generally reduced. Therefore, although it seems that a field of more than 250 mV/Å is needed to perform atom migration in our calculations, a relatively small bias voltage (50–100 mV) is needed to trigger the atom movement in our experiments.

IV. CONCLUSIONS

In order to accurately fabricate an atom-sized gap, a strategy of the FAAM method based on MCBJ technology is developed in this paper both theoretically and experimentally. To understand the mechanism of atom-sized gap fabrication, the probable configuration evolutions are investigated in the stretching and compressing processes of a gold nanojunction based on the *ab initio* calculations. The calculations show that, although various kinds of configuration evolutions may take place in different stretching and compressing processes, the standard lattice configuration is still the most stable configuration. The conductance traces, force traces, and stiffness factors in the stretching and compressing processes are further discussed, which can provide significant information to fulfill the task of fabricating a single-atom-sized gap by FAAM using a gold nanojunction. The vacant position produced in the stretching process makes it feasible for atom migration. The most probable dimension of the gap produced by field-induced atom migration is 0.32–0.40 nm. Based on our theoretical scheme, we successfully fabricate one-atom-sized gaps with high yields via an experiment by applying the MCBJ-based FAAM method.

ACKNOWLEDGMENTS

This work was supported by the National Natural Science Foundation of China (Grants No. 11374195, No. 21303171, No. 61571242, and No. 11704230), the Natural Science Foundation of Shandong Province, China (Grant No. ZR2018MA037), and the Postdoctoral Science Foundation (Grant No. 2017M612321) of China. We thank the Taishan Scholar Project of Shandong Province and the Key Laboratory of Medical Physics and Image Processing Technology of Shandong Province for the support.

[1] M. A. Reed, C. Zhou, C. J. Muller, T. P. Burgin, and J. M. Tour, Conductance of a molecular junction, Science **278**, 252 (1997).

[2] X. D. Cui, A. Primak, X. Zarate, J. Tomfohr, O. F. Sankey, A. L. Moore, T. A. Moore, D. Gust, G. Harris, and S. M. Lindsay, Reproducible measurement of single-molecule conductivity, Science **294**, 571 (2001).

[3] Z. L. Li, B. Zou, C. K. Wang, and Y. Luo, Electronic transport properties of molecular bipyridine junction: Effects of isomer and contact structures, Phys. Rev. B **73**, 075326 (2006).

[4] M. Sun, Z. Zhang, H. Zheng, and H. Xu, *In situ* plasmon-driven chemical reactions revealed by high vacuum tip-enhanced Raman spectroscopy, Sci. Rep. **2**, 647 (2012).

[5] Y. Yang, Z. B. Chen, J. Y. Liu, M. Lu, D. Z. Yang, F. Z. Yang, and Z. Q. Tian, An electrochemically assisted mechanically controllable break junction approach for single molecule junction conductance measurements, Nano Res. **4**, 1199 (2011).

[6] X. X. Fu, R. Q. Zhang, G. P. Zhang, and Z. L. Li, Rectifying properties of oligo(phenylene ethynylene) heterometallic molecular junctions molecular length and side group effects, Sci. Rep. **4**, 6357 (2014).

[7] E. Zerah-Harush and Y. Dubi, Enhanced Thermoelectric Performance of Hybrid Nanoparticle-Single-Molecule Junctions, Phys. Rev. Applied **3**, 064017 (2015).

[8] B. Q. Xu, X. L. Li, X. Y. Xiao, H. Sakaguchi, and N. J. Tao, Electromechanical and conductance switching properties of single oligothiophene molecules, Nano Lett. **5**, 1491 (2005).

[9] Z. L. Li, J. J. Bi, R. Liu, X. H. Yi, H. Y. Fu, F. Sun, M. Z. Wei, and C. K. Wang, Gas-sensor property of single-molecule device: F_2 adsorbing effect, Chin. Phys. B **26**, 098508 (2017).

[10] S. J. van der Molen, R. Naaman, E. Scheer, J. B. Neaton, A. Nitzan, D. Natelson, N. J. Tao, H. van der Zant, M. Mayor, M. Ruben, M. Reed, and M. Calame, Visions for a molecular future, Nat. Nanotechnol. **8**, 385 (2013).

[11] M. Ratner, A brief history of molecular electronics, Nat. Nanotechnol. **8**, 378 (2013).

[12] S. Y. Quek, M. Kamenetska, M. L. Steigerwald, H. J. Choi, S. G. Louie, M. S. Hybertsen, J. B. Neaton, and L. Venkataraman, Mechanically controlled binary conductance switching of a single-molecule junction, Nat. Nanotechnol. **4**, 230 (2009).

[13] F. Chen, J. He, C. Nuckolls, T. Roberts, J. E. Klare, and S. Lindsay, A molecular switch based on potential-induced changes of oxidation state, Nano Lett. **5**, 503 (2005).

[14] A. S. Blum, J. G. Kushmerick, D. P. Long, C. H. Patterson, J. C. Yang, J. C. Henderson, Y. Yao, J. M. Tour, R. Shashidhar, and B. R. Ratna, Molecularly inherent voltage-controlled conductance switching, Nat. Mater. **4**, 167 (2005).

[15] E. Lörtscher, J. W. Ciszek, J. Tour, and H. Riel, Reversible and controllable switching of a single-molecule junction, Small **2**, 973 (2006).

[16] P. Liljeroth, J. Repp, and G. Meyer, Current-induced hydrogen tautomerization and conductance switching of naphthalocyanine molecules, Science **317**, 1203 (2007).

[17] C. C. Jia, B. J. Ma, N. Xin, and X. F. Guo, Carbon electrode-molecule junctions: A reliable platform for molecular electronics, Acc. Chem. Res. **48**, 2565 (2015).

[18] J. Hodgkiss, E. Zysman-Colman, S. Higgins, G. Solomon, I. Bâldea, I. Samuel, L. Venkataraman, F. Wudl, B. Xu, R. Venkatramani, H. Ottosson, D. Perepichka, U. Lemmer, P. Skabara, A. Mount, and D. Bradley, Molecular electronics: General discussion, Faraday Discuss. **174**, 125 (2014).

[19] O. Ivashenko, A. J. Bergren, and R. L. McCreery, Light emission as a probe of energy losses in molecular junctions, J. Am. Chem. Soc. **138**, 722 (2016).

[20] Y. Kim, W. Jeong, K. Kim, W. Lee, and P. Reddy, Electrostatic control of thermoelectricity in molecular junctions, Nat. Nanotechnol. **9**, 881 (2014).

[21] B. Kim, S. H. Choi, X. Y. Zhu, and C. D. Frisbie, Molecular tunnel junctions based on pi-conjugated oligoacene thiols and dithiols between Ag, Au, and Pt contacts: Effect of surface linking group and metal work function, J. Am. Chem. Soc. **133**, 19864 (2011).

[22] C. C. Bof Bufon, J. D. Arias Espinoza, D. J. Thurmer, M. Bauer, C. Deneke, U. Zschieschang, H. Klauk, and O. G. Schmidt, Hybrid organic/inorganic molecular heterojunctions based on strained nanomembranes, Nano Lett. **11**, 3727 (2011).

[23] F. Schwarz, G. Kastlunger, F. Lissel, C. Egler-Lucas, S. N. Semenov, K. Venkatesan, H. Berke, R. Stadler, and E. Lörtscher, Field-induced conductance switching by charge-state alternation in organometallic single-molecule junctions, Nat. Nanotechnol. **11**, 170 (2016).

[24] D. Xiang, X. Wang, C. Jia, T. Lee, and X. Guo, Molecular-scale electronics: From concept to function, Chem. Rev. **116**, 4318 (2016).

[25] C. A. Martin, R. H. M. Smit, H. S. J. van der Zant, and J. M. van Ruitenbeek, A nanoelectromechanical single-atom switch, Nano Lett. **9**, 2940 (2009).

[26] D. L. Bao, R. Liu, J. C. Leng, X. Zuo, Y. Jiao, Z. L. Li, and C. K. Wang, Theoretical study on mechanical and electron-transport properties of conjugated molecular junctions with carboxylic or methyl sulfide links, Phys. Lett. A **378**, 1290 (2014).

[27] Z. L. Li, G. P. Zhang, and C. K. Wang, First-principles study on formation and electron transport properties of single oligothiophene molecular junctions, J. Phys. Chem. C **115**, 15586 (2011).

[28] H. Song, Y. Kim, Y. H. Jang, H. Jeong, M. A. Reed, and T. Lee, Observation of molecular orbital gating, Nature (London) **462**, 1039 (2009).

[29] C. C. Jia, A. Migliore, N. Xin, S. Y. Huang, J. Y. Wang, Q. Yang, S. P. Wang, H. L. Chen, D. M. Wang, B. Y. Feng, Z. R. Liu, G. Y. Zhang, D. H. Qu, H. Tian, M. A. Ratner, H. Q. Xu, A. Nitzan, and X. F. Guo, Covalently bonded single-molecule junctions with stable and reversible photoswitched conductivity, Science **352**, 1443 (2016).

[30] D. Natelson, Mechanical break junctions enormous information in a nanoscale package, ACS Nano **6**, 2871 (2012).

[31] S. V. Aradhya, M. Frei, M. S. Hybertsen, and L. Venkataraman, Van der Waals interactions at metal/organic interfaces at the single-molecule level, Nat. Mater. **11**, 872 (2012).

[32] L. Venkataraman, J. E. Klare, C. Nuckolls, M. S. Hybertsen, and M. L. Steigerwald, Dependence of single-molecule junction conductance on molecular conformation, Nature (London) **442**, 904 (2006).

[33] L. Venkataraman, J. E. Klare, I. W. Tam, C. Nuckolls, M. S. Hybertsen, and M. L. Steigerwald, Single-molecule circuits with well-defined molecular conductance, Nano Lett. **6**, 458 (2006).

[34] Q. Wang, R. Liu, D. Xiang, M. Sun, Z. Zhao, L. Sun, T. Mei, P. Wu, H. Liu, X. Guo, Z. L. Li, and T. Lee, Single-atom switches and single-atom gaps using stretched metal nanowires, ACS Nano **10**, 9695 (2016).

[35] C. Schirm, M. Matt, F. Pauly, J. C. Cuevas, P. Nielaba, and E. A. Scheer, Current-driven single-atom memory, Nat. Nanotechnol. **8**, 645 (2013).

[36] F. Q. Xie, R. Maul, A. Augenstein, C. Obermair, E. B. Starikov, G. Schön, T. Schimmel, and W. Wenzel, Independently switchable atomic quantum transistors by reversible contact reconstruction, Nano Lett. **8**, 4493 (2008).

[37] T. Kizuka, S. Kodama, and T. Matsuda, Verification of unzipping models of electromigration in gold nanocontacts by *in situ* high-resolution transmission electron microscopy, Nanotechnology **21**, 495706 (2010).

[38] K. H. Bevan, H. Guo, E. D. Williams, and Z. Zhang, First-principles quantum transport theory of the enhanced wind force driving electromigration on Ag(111), Phys. Rev. B **81**, 235416 (2010).

[39] M. Brandbyge, K. Stokbro, J. Taylor, J. L. Mozos, and P. Ordejón, Origin of current-induced forces in an atomic gold wire: A first-principles study, Phys. Rev. B **67**, 193104 (2003).

[40] R. Zhang, I. Rungger, S. Sanvito, and S. Hou, Current-induced energy barrier suppression for electromigration from first principles, Phys. Rev. B **84**, 085445 (2011).

[41] R. Liu, C. K. Wang, and Z. L. Li, A method to study electronic transport properties of molecular junction: One-dimension transmission combined with three-dimension correction approximation (OTCTCA), Sci. Rep. **6**, 21946 (2016).

[42] R. Liu, D. L. Bao, Y. Jiao, L. W. Wan, Z. L. Li, and C. K. Wang, Study on force sensitivity of electronic transport properties of 1,4-butanedithiol molecular device, Acta Phys. Sin. **63**, 068501 (2014).

[43] M. J. Frisch *et al.* GAUSSIAN 03, revision A.1, Gaussian, Inc., 2003.

[44] M. Buttiker, Y. Imry, R. Landauer, and S. Pinhas, Generalized many-channel conductance formula with application to small rings, Phys. Rev. B **31**, 6207 (1985).

[45] J. P. Perdew, K. Burke, and M. Ernzerhof, Generalized Gradient Approximation Made Simple, Phys. Rev. Lett. **77**, 3865 (1996).

[46] M. Frei, S. V. Aradhya, M. Koentopp, M. S. Hybertsen, and L. Venkataraman, Mechanics and chemistry: Single molecule bond rupture forces correlate with molecular backbone structure, Nano Lett. **11**, 1518 (2011).

[47] B. Xu and N. J. Tao, Measurement of single-molecule resistance by repeated formation of molecular junctions, Science **301**, 1221 (2003).

[48] S. V. Aradhya, J. S. Meisner, M. Krikorian, S. Ahn, R. Parameswaran, M. L. Steigerwald, C. Nuckolls, and L. Venkataraman, Dissecting contact mechanics from quantum interference in single-molecule junctions of Stilbene derivatives, Nano Lett. **12**, 1643 (2012).

[49] J. Zhao, K. Murakoshi, X. Yin, M. Kiguchi, Y. Guo, N. Wang, S. Liang, and H. Liu, Dynamic characterization of the postbreaking behavior of a nanowire, J. Phys. Chem. C **112**, 20088 (2008).

[50] D. Weckbecker, P. B. Coto, and M. Thoss, Controlling the conductance of a graphene-molecule nanojunction by proton transfer, Nano Lett. **17**, 3341 (2017).

[51] D. Xiang, H. Jeong, T. Lee, and D. Mayer, Mechanically controllable break junctions for molecular electronics, Adv. Mater. **25**, 4845 (2013).

[52] Z. Zhao, R. Liu, D. Mayer, M. Coppola, L. Sun, Y. Kim, C. K. Wang, L. Ni, M. Wang, Z. L. Li, T. Lee, and D. Xiang, Shaping the atomic-scale geometries of electrodes to control optical and electrical performance of molecular devices, Small **14**, 1703815 (2018).

[53] D. Xiang, H. Jeong, D. Kim, T. Lee, Y. Cheng, Q. Wang, and D. Mayer, Three-terminal single-molecule junctions formed by mechanically controllable break junctions with side gating, Nano Lett. **13**, 2809 (2013).

[54] D. Xiang, Y. Zhang, F. Pyatkov, A. Offenhäusser, and D. Mayer, Gap size dependent transition from direct tunneling to field emission in single molecule junctions, Chem. Commun. (Cambridge) **47**, 4760 (2011).

[55] Z. M. Wu, M. Steinacher, R. Huber, M. Calame, S. J. van der Molen, and C. Schönenberger, Feedback controlled electromigration in four-terminal nanojunctions, Appl. Phys. Lett. **91**, 053118 (2007).

[56] A. Umeno and K. Hirakawa, Spectroscopic analysis of electromigration at gold nanojunctions, Physica (Amsterdam) **42E**, 2826 (2010).

[57] Y. Naitoh, T. Ohata, R. Matsushita, E. Okawa, M. Horikawa, M. Oyama, M. Mukaida, D. F. Wang, M. Kiguchi, K. Tsukagoshi, and T. Ishida, Self-aligned formation of sub 1 nm gaps utilizing electromigration during metal deposition, ACS Appl. Mater. Interfaces **5**, 12869 (2013).